JOURNAL OF MECHANICS IN MEDICINE AND BIOLOGY

ISSN (print): 0219-5194 | ISSN (online): 1793-6810

https://www.worldscientific.com/worldscinet/jmmb

IMPACT FACTOR = 0.883

Accepted July 18th 2022

MATHEMATICAL MODELLING OF THERMO-SOLUTAL TRANSPORT IN PULSATING FLOW IN THE HYDROCEPHALUS

Hemalatha Balasundaram[1]*, Senthamilselvi Sathiamoorthy[2]

Department of Mathematics, Vels Institute of science, Technology and Advanced Studies Chennai, Tamil Nādu. ***India.***

O. Anwar Bég[2]

Professor and Director- Multi-Physical Engineering Sciences Group, Dept. Mechanical and Aeronautical Engineering, SEE, Salford University, Manchester, M54WT, ***UK.***

Corresponding author: hemalatha.phd@velsuniv.ac.in

ABSTRACT

Cerebrospinal fluid (CSF) is a symmetric flow transport that surrounds brain and central nervous system (CNS). Hydrocephalus is an asymmetric and unusual cerebrospinal fluid flow in the lateral ventricular portions. This dumping impact enhances the elasticity over the ventricle wall. Henceforth, compression change influences the force of brain tissues. Mathematical models of transport in the hydrocephalus which constitutes an excess of fluid in the cavities deep within the brain, enable a better perspective of how this condition contributes to disturbances of the cerebrospinal fluid (CSF) flow in the hollow places of the brain. Recent approaches to brain phase spaces reinforce the foremost role of symmetries and energy requirements in the assessment of nervous activity. Thermophysical and mass transfer effects are therefore addressed in the present article to quantify the transport phenomena in pulsatile hydrocephalus CSF transport with oscillating pressure variations that characterize general neurological activity and transitions from one functional state to another. A new mathematical model is developed which includes porous media drag for brain tissue and solutal diffusion (concentration) effects. A classical Laplace transform method is deployed to solve the dimensionless model derived with appropriate boundary conditions. The analysis reveals that with increasing permeability of the subarachnoid space, the CSF velocity is increased, and a significant fluid flux enhancement arises through the brain parenchyma as the pressure of the fluid escalates drastically due to hydrocephalus disorder. Stronger thermal buoyancy (Grashof number) also results in deceleration in the flow. CSF temperature is reduced with progression in time. Particle (e. g. ion) concentration is suppressed with increasing Schmidt number. As heat conduction parameter increases there is a substantial depletion in CSF velocity with respect to time. Increasing Womersley parameter

displaces the CSF velocity peaks and troughs. The present effects are beneficial in determining the thermo-fluidic transport mechanism of the pathological disorder hydrocephalus. Also, the present results are compared with those clinical studies for some cases. we have confirmed that our validity provides a decent justification with the neurological studies.

KEYWORDS: *Cerebrospinal fluid, heat transfer, Pulsatile inlet velocity, Brain Parenchyma, oscillating pressure, Laplace transforms, Hydrocephalus, Grashof number, Schmidt number.*

NOMENCLATURE

$CSF \longmapsto Cerebrospinal\ Fluid$

$u_c, v_c \longmapsto dimensionless\ velocity\ components\ for\ CSF$ in x and y directions

$u_c^*, v_c^* \longmapsto dimensional\ velocity\ components\ for\ CSF\ flow$ in x^* and y^* directions.

$CNS \longmapsto Cental\ nervous\ system$

$ICP \longmapsto Intracranial\ pressure$

$SAS \longmapsto Subarachnoid\ Space$

$\rho \longmapsto fluid\ density$

$\nu \longmapsto kinematic\ viscosity$

$k_m * \longmapsto permeabilty\ of\ porous\ layer\ (pia\ mater)$

$U_0 \longmapsto$ Characteristic velocity

$\alpha^2 \longmapsto Womersely\ number$

$\lambda \longmapsto oscillating\ parameter$

$c_p \longmapsto Specific\ heat\ \ capacity\ at\ constant\ pressure$

$T_w \longmapsto$ Wall temperature of pia mater

$C_w \longmapsto$ Wall concentration of CSF flow

$T_\infty \longmapsto Ambient$ temperature of CSF flow

$C_0 \longmapsto Ambient$ concentration of CSF flow

$Re \longmapsto Reynolds\ Number$

$J \longmapsto Heat\ conduction\ parameter$

$k \longmapsto\ thermal\ conductivity$

$K_T \mapsto thermal\ diffusion\ ratio$

$t \longmapsto dimensionless\ time$

$\sigma^2 \longmapsto Permeability\ parameter$

$g \longmapsto acceleration\ due\ to\ gravity$

$Gc \longmapsto Grashof\ number\ for\ mass\ transfer$

$Gr \longmapsto Grashof\ number\ for\ heat\ transfer$

$Pr \longmapsto Prandtl\ number$

$R \longmapsto Resistance\ of\ fluid\ flow$

$N \longmapsto Number\ density\ of\ fluid\ flow$

$Sc \longmapsto Schmidt\ number$

$\theta_c \longmapsto Temperature\ of\ fluid$

$C \longmapsto transport\ diffusivity\ of\ the\ fluid$

$x\ and\ y \mapsto Cartesian\ Coordinates$

1. INTRODUCTION

Transport phenomena in the human brain is a growing area of modern biomechanics which features multiple criteria including porous media, viscous flow, heat transfer, mass transfer, elasticity etc. In the past two decades, fluid dynamics has contributed increasingly to improve clinical understanding of cerebral behaviour. An important ailment in brain physiology is congenital hydrocephalus, a pathological condition in which the normal flow of the cerebrospinal fluid is disturbed, causing the brain to become deformed. This condition constitutes an asymmetric and unusual cerebrospinal fluid flow during fetal development. In this condition, the surplus cerebrospinal fluid (CSF) induces elastic deformations and compression change, influencing the brain tissues. Mathematical models of transport in the hydrocephalus which constitutes an excess of fluid in the cavities deep within the brain, enable a better perspective of how this condition contributes to disturbances of the cerebrospinal fluid (CSF) flow in the hollow places of the brain. Thermal and pulsating effects are very important in cerebrospinal transport. Hydrocephalic patients are growing worldwide and there is a need to further elucidate the interaction of thermal, solutal (mass transfer) and hydrodynamic effects to develop more effective treatments. Therefore, motivated by exploring in more detail the physiological transport in hydrocephalus, which enables a deeper understanding of this condition, it is important to simulate the temperature effects on pulsatile hydrocephalus CSF flow and how these influence oscillating pressure. To achieve this goal, fluid movement along the subarachnoid space passing through the central nervous system requires the pulsatile flow dynamics to include thermal effects ie.,

thermal conduction and convective heat transfer, in addition to porous media characteristics of the brain tissue, mass transfer (solutal) and other phenomena. In recent years a number of investigators have explored both experimentally and numerically various thermal and flow aspects of hydrocephalus CSF. Hirashima *et al*.,[1] reported on brain temperature measurements at various depths beneath the pial surface in hydrocephalus patients of varying aetiology, noting that temperature increased gradually with depth in all patients, with the maximum temperature observed in the ventricle. Rajasekaran *et al*. [2] used a thermal time of flight method to quantify the cerebrospinal fluid flow rate in hydrocephalus shunts, by deploying a modified shunt tube system covered with artificial skin for thermal behaviour. They recorded velocity and flow rate of the cerebrospinal fluid by decoupling the thermal transfer in the measured differential time at two measurement spots and also validated a finite element analysis on the fluidic and thermal behaviors of the shunt system. They observed good correlation between simulation and measurements in the clinically practical flow rate range of 0.5 mm/sec to 1.0 mm/sec. Madsen [3] developed a new non-invasive device (Shunt check) to detect cerebrospinal fluid (CSF) flow in a shunt by sensing skin temperature downstream from a region of CSF in hydrocephalic patients. They also conducted a statistical analysis (Fisher's test) on 100 patients, including 48 evaluated during possible shunt malfunction, of whom 24 went on to surgical exploration. Neff [4] conducted noninvasive transcutaneous thermal convection CSF shunt flow measurements, developing an approach which improves on brain imaging and radionuclide shunt studies. Herbowski and Gurgul [5] conducted experiments based on a thermodynamic approach to study cerebrospinal fluid circulation, using skin temperature measurement differences between the frontal and lumbar spinal regions. They emphasized that temperature difference between both ends of the subarachnoid space in the intracranial and the intracanal compartments may induce natural circulation of cerebrospinal fluid to attain a thermal equilibrium and the Brownian motions are the driving forces for the upward cerebrospinal fluid bulk flow, whereas gravity is the driving force for the downward cerebrospinal fluid bulk flow. Other studies of brain transport phenomena have utilized thermodynamic (entropy) approaches including Déli and Kisvárday [6] who simulated the brain as a thermodynamic cycle of perception that can be modeled by the Carnot engine. They showed that different entropy levels are relatable to different emotional states in the brain. Donnelly and Czosnyka [7] also analyzed the brain as a thermodynamic system, showing that blood flow acts effectively as a cooler for the brain. They also considered cerebral blood flow and volume, intracranial pressure and other aspects from a thermal view point, noting that blood is cooler normally than the cerebrum tissue temperature, and outflowing venous blood is typically hotter than the blood vessel but cooler than the

neural tissue. Zakharov and Sadovsky[8] developed a non-equilibrium second law (entropy) thermodynamic model for the role of circulating blood in temperature control in homeothermic creatures. Their model produced a direct relationship between skin and climate temperatures. Gholampour *et al.* [9] presented 3-D hydro-elastic numerical simulations of the interaction of cerebrospinal fluid (CSF) and cerebrum tissue in hydrocephalus patients, both before and after shunting. It was noted that CSF mean pressure and pressure amplitude (for non-communicating hydrocephalus) are both several times greater at least in hydrocephalus patients compared with healthy subjects. Keong *et al.* [10] deployed diffusion tensor imaging (DTI) to determine the topography and reversibility of white matter injury in normal pressure hydrocephalus (NPH) pre- and early after shunting. McAllister *et al.* [11] emphasized a number of critical areas for further research into hydrocephalus patients including causes (absorption, production, and related drug therapies), macromolecular (mass) transport mechanisms, thermal effects, biomechanical changes in hydrocephalus and age-dependent mechanisms in the development of hydrocephalus. Smillie *et al.* [12] presented numerical simulations of poro-elastic flow in the hydrocephalus. They extended previous studies by including flow through the aqueduct via more anatomically viable boundary conditions. They deployed a two-layered model for white and grey matter to better represent cerebral materials. Zhu *et al.* [13] developed quantitative MRI techniques to measure, model and visualize cerebrospinal fluid (CSF) hydrodynamics in both normal subjects and hydrocephalic patients. Tangen *et al*. [14] used computational fluid dynamics (CFD) to simulate the micro-anatomical effects on cerebrospinal fluid (CSF) flow patterns and flow resistance within the entire central nervous system (CNS) using reconstructed geometric models. They showed that nerve roots and trabeculae generate complex zones of microcirculation along the spine and that drug dispersion is boosted by pulsatile flow around microanatomy-induced vortices. Gholampour [15] used ADINA finite element software to simulate the fluid structure interaction in non-communicating hydrocephalus (NCH) geometries. He showed that the evaluation of ventricles volume and maximum CSF pressure (before shunting) are the dominant hydrodynamic indices for characterizing the flow and that the maximum CSF pressure is the most sensitive parameter to clinical symptoms. He also computed the phase lag between flow rate and pressure gradient functions and the degree of CSF pulsatility. H Balasundaram *et al*. [16] illustrated a mathematical study of flow and mass transfer in the congenital hydrocephalus with the effects of ventricular elasticity and chemical reaction using a simple porous medium model. They derived perturbation solutions for the dimensionless conservation equations with associated boundary conditions and showed that with increasing elastic (Young's) modulus parameter and

Reynolds number, CSF flow is accelerated. They also noted that concentration is enhanced with Péclet number and that the CSF flow is accelerated with Darcy (permeability) number.

Although many other studies of transport in both communicating and non-communicating hydrocephalus models have been presented by Gholampour [17-19], Malm *et al.* [20], Linninger *et al.* [21] and Sweetman *et al.* [22], these have been restricted to only viscous flow and have neglected heat and mass transfer that is, thermo-solutal effects. As noted earlier, thermal and mass (molecular) diffusion have a significant role to play in CSF transport generally. Therefore, in the present study a mathematical model is developed to consider the pulsatile flow in a porous medium model of the hydrocephalus with combined heat and mass transfer. Thermal and mass (solutal) buoyancy effects are included. Darcy's model is deployed for the pia matter (porous medium). The non-dimensional model is solved using Laplace transforms with error functions [23]. [24-28], investigated the convective Darcy–Forchheimer flow of nano particle over an energy and solutal reaction. Graphical results are then presented with clinically viable data using MATLAB symbolic software for the influence of selected emerging transport parameters e.g., Darcy permeability number, Schmidt number, thermal Grashof number, Womersley number, heat conduction parameter etc., on pulsatile flow velocity, temperature and concentration distributions. The present study while using a simple geometric model provides a new direction in multi-physical transport phenomena in the hydrocephalus and furthermore a benchmark for more geometrically complex simulations with computational fluid dynamics (CFD) codes.

2. MATHEMATICAL MODEL FOR THERMOSOLUTAL HYDROCEPHALUS TRANSPORT

CSF is a watery fluid that protects the brain that passes through the spinal cord. CSF is formed mainly by two lateral ventricles next to the brain parenchyma pia mater. As hydrocephalus results in excessive secretion of volumes of CSF, a surplus in CSF fluid moves in the subarachnoid space (SAS). It is assumed in the present model that CSF is an isothermal and incompressible Newtonian fluid.

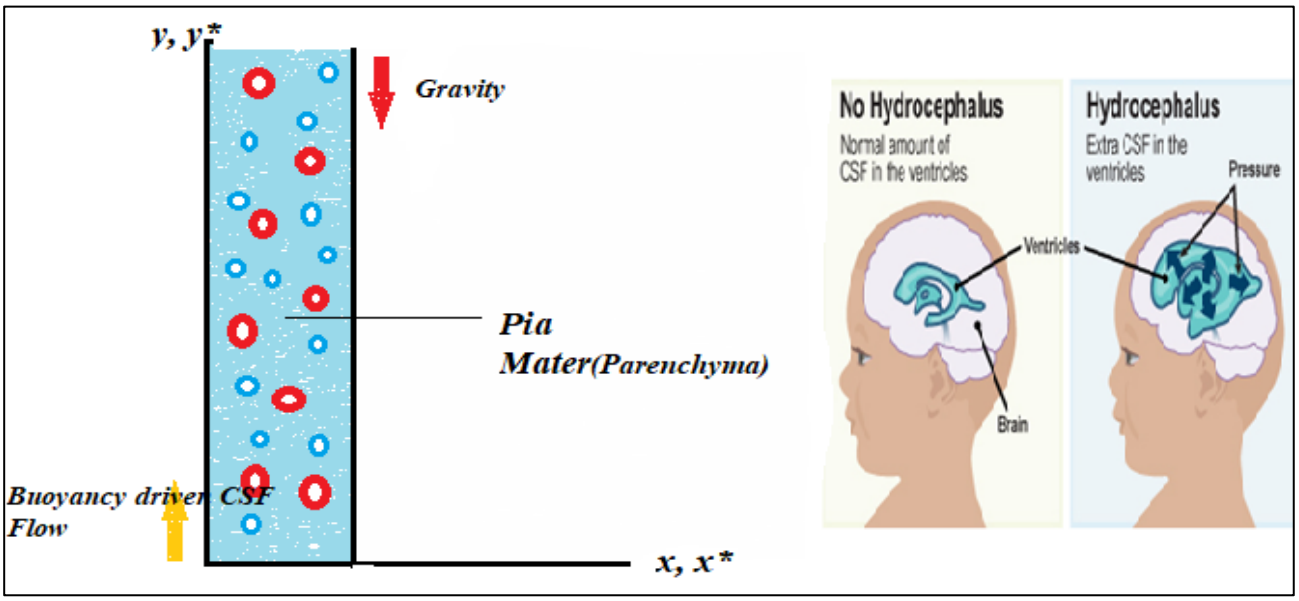

Fig: 1 Hydrocephalus and idealized geometrical model for transport

The density and viscosity of its flow are considered to be $1000\,kg/m^3$ and $0.001\,kg/ms$. The physical model is shown in **Fig. 1**. A Cartesian coordinate system (x^*, y^*), is adopted, where x^* is transverse coordinate and y^* is the vertical coordinate. The fluid is maintained no slip on the walls of subarachnoid space at the constant concentration $C_w{}^*$,temperature $T_w{}^*$ higher than the ambient temperature T_∞ and ambient concentration C_0 respectively. The rest of the properties of CSF fluid are assumed to be constant. To reduce the analysis of independent parameters we assume:(a) neglect body forces are considered as constant except the density variation in the buoyancy term. The temperature difference and concentration differences generate thermal and solutal buoyancy forces in the CSF. (b) The pressure exerted in the fluid is therefore oscillating with respect to time. (c) unsteady pulsatile CSF flow with hydraulic temperature and mass diffusion in a Darcian porous medium brain parenchyma is considered even though, the porous medium is isotropic and homogenous for the pia matter. (d) The surface of the CSF flow is embedded in a highly porous medium called brain parenchyma. (e) Neglecting electro-magnetic field strength, the brain fluid.

Consideration these assumptions, the equations governing the transport are the mass, momentum, energy (heat) and solute conservation with the Boussinesq approximation and boundary layer assumption for the Newtonian CSF flow is represented as follows:

Mass conservation [21]

$$\frac{\partial u_c{}^*}{\partial x^*} + \frac{\partial v_c{}^*}{\partial y^*} = 0 \qquad (1)$$

Momentum conservation [21] with some source terms added.

$$\frac{\partial u_c^*}{\partial t^*} = -\frac{1}{\rho}\frac{\partial P_c^*}{\partial t^*} + \nu\left(\frac{\partial^2 u_c^*}{\partial y^{*2}}\right) + g\beta_T(T_c^* - T_\infty^*) + g\beta_C(C_c^* - C_\infty^*) + \frac{RN}{\rho}u_c^* - \frac{\nu}{k_m^*}u_c^* \quad (2)$$

Energy Conservation [4]

$$\left(\frac{\partial T_c^*}{\partial t^*}\right) = \frac{k_T}{\rho C_p}\left(\frac{\partial^2 T_c^*}{\partial y^{*2}}\right) - J(T_c^* - T_\infty^*) \quad (3)$$

Concentration (Solute) Conservation [29]

$$\left(\frac{\partial C_c^*}{\partial t^*}\right) = D\left(\frac{\partial^2 C_c^*}{\partial y^{*2}}\right) \quad (4)$$

The spatial and temporal boundary conditions are prescribed as:

$$\left.\begin{aligned} &u_c^* = 0\,, C_c^* = C_\infty^*\ and\ T_c^* = T_\infty^*\ for\ y^* \geq 0, x^* > 0,\ t^* \leq 0 \\ &u_c^* = h\,Cos\omega t^*\,, C_c^* = C_w^*\ and\ T_c^* = T_w^*\ at\ y^* = 0 \\ &u_c^* = 0, C_c^* \to C_\infty^*\ and\ T_c^* = T_\infty^*\ at\ y^* \to \infty \qquad t > 0 \end{aligned}\right\} \quad (5)$$

All parameters are defined in the nomenclature. It is useful to introduce dimensionless quantities which are defined as follows:

$$x = \frac{x^*}{h_p}\,,\ y = \frac{y^* U_0}{\nu}, u_c = \frac{u_c^*}{U_0}\ , \theta_c^* = \frac{T_c^* - T_\infty^*}{T_w^* - T_\infty^*}\ , \quad (6)$$

$$C^* = \frac{C_c^* - C_\infty^*}{C_w^* - C_\infty^*}\ ,\ P = \frac{P_c^*}{\rho {U_0}^2} \qquad t = \frac{t^* {v_0}^2}{\nu}\ , \propto^2 = \frac{\omega l^2}{\nu}$$

Here, $u_c^*, T_c^*,\ C_c^*, P_c^*$represents the dimensional components of fluid velocity, temperature, concentration, and pressure respectively. $x^*,\ y^*, t^*$indicates the dimensional coordinates, time taken, g denotes the gravitational force. β_C and β_T identifies the coefficients of solutal and thermal expansion. $T_w^*\ and\ C_w^*$ denotes wall temperature and concentration, T_∞^* denotes ambient temperature. t is dimensionless time. R, N denotes the resistance and number density. $C_p$represents specific heat. D indicats the mass diffusivity coefficient. x and y are dimensionless

coordinates. u_c, C, θ_c represents dimensionless fluid velocity, concentration of solute and temperature of hydrocephalus. G_{pv} is the resistance parameter. U_0 denotes the characteristic velocity of the fluid. P is dimensionless pressure. $\propto^2$ represents the Womersley number (ratio of transient inertial force to viscous force) which quantifies the pulsatile nature of the CSF flow in hydrocephalus and ω is frequency of oscillatory (pulsatile) motion.

The transverse pressure gradient decays exponentially with time in CSF flow in the regime. Implementing Eqn. (6) in Eqns. (1)-(5) yields the following system of dimensionless coupled partial differential equations:

$$\frac{\partial u_c}{\partial t} = -\frac{\partial P}{\partial x} + \left(\frac{\partial^2 u_c}{\partial y^2}\right) - \sigma^2 u_c + \frac{G_{pv}}{Re^2} u_c + Gr\theta_c + GcC \tag{7}$$

$$\frac{\partial \theta_c}{\partial t} = \frac{1}{Pr}\frac{\partial^2 \theta_c}{\partial y^2} - J\theta_c \tag{8}$$

$$\frac{\partial C}{\partial t} = \frac{1}{Sc}\frac{\partial^2 C}{\partial y^2} \tag{9}$$

In Eqn. (7), $-\frac{\partial P}{\partial x} = e^{-\lambda t}$ ~~and~~ expresses the exponentially decaying transverse pressure gradient. Furthermore, the dimensionless numbers in Eqns. (7)-(9) take the definitions:

$Gr = \frac{g\beta_T(T_w{}^* - T_\infty{}^*)\nu}{U_0{}^3}$ [Grashof number];

$Gc = \frac{g\beta_{TC}(C_w{}^* - C_\infty{}^*)\nu}{U_0{}^3}$ [Mass Grashof number];

$\sigma^2 = \frac{\nu^2}{U_0{}^2 k_m{}^*}$ [Darcy permeability number];

$\mathrm{R}e = \frac{hu_c}{\nu}$ [Reynolds Number];

$Pr = \frac{\mu C_p}{k_T}$ [Prandtl number];

$G_{pv} = \frac{R\,N\,h^2}{\mu}$ [Particle mass number].

$Sc = \frac{\nu}{D}$ [Schmidt number]. (10)

Here 'h' is an arbitrary length. The transformed boundary conditions become:

$$\left.\begin{aligned} &u_c = 0 \; as \; y \to \infty \\ &u_c = Cos \propto^2 t \; as \; y \to 0 \\ &\theta_c = 0 \;\; at \; y \geq 0, C = 0 \;\; at \; y \geq 0 \\ &\theta_c = 0 \, , C = 0 \; as \; y \to \infty \\ &\theta_c = 1 \, , C = 1 \; as \; y = 0 \end{aligned}\right\} \qquad (11)$$

3. ANALYTICAL SOLUTIONS

The mathematical model derived and defined by Eqns. (7)-(9) and boundary conditions (11) is solved with a classical Laplace technique and its inverse transforms [23]. Solutions are derived for the CSF velocity, temperature and concentration functions, using the following transforms:

Taking Laplace transform of both sides of Eqns .(7),(8),(9), we get the results as follows

$$D^2 L(c) - (Sc + s)L(c) = 0$$

$$c = L^{-1}\left[\frac{e^{-y\sqrt{(Sc\,S)}}}{s}\right]$$

$$D^2 L(\theta) - (J + s)L(\theta) = 0$$

$$\theta = L^{-1}\left[\frac{e^{-y\sqrt{(J+s)Pr}}}{s}\right]$$

$$D^2 L(u_c) - \frac{1}{\sigma^2} L(u_c) - sL(u_c) = \frac{-1}{s+\lambda} - GrL(\theta) - Gm\, L(c) + \frac{G_{pv}}{Re^2} L(u_c)$$

$$u_c = L^{-1}\left[e^{-\sqrt{k+s}}\left(\frac{s}{s^2+\beta^2} - \frac{1}{k+\lambda}\left(\frac{1}{s-k} - \frac{1}{s-\lambda}\right) + \frac{Gr}{R}\left(\frac{1}{s} - \frac{1-Pr}{R+(Pr-1)s}\right)\right.\right.$$
$$\left.\left. - \frac{Gm}{k}\left(\frac{1}{s} - \frac{Sc-1}{K-(Sc-s)s}\right)\right) + L^{-1}\left[\frac{1}{k+\lambda}\left(\frac{1}{s-k} - \frac{1}{s-\lambda}\right)\right]\right.$$
$$- \frac{Gr}{R}L^{-1}\left(\frac{e^{-y\sqrt{(J+s)Pr}}}{s} - \frac{e^{-y\sqrt{(J+s)Pr}}(Pr-1)}{R+(Pr-1)s}\right)$$
$$\left. + \frac{Gm}{k}L^{-1}\left(\frac{e^{-y\sqrt{(Sc\,S)}}}{s} - \frac{e^{-y\sqrt{(Sc\,S)}}(Sc-1)}{k-(Sc-1)s}\right)\right]$$

Using the formula in [23], we get

$$L(u_c) = e^{-y\sqrt{k+s}}\left[\frac{s}{s^2+\beta^2} - \frac{1}{k+\lambda}\left[\frac{1}{s-k} - \frac{1}{s+\lambda}\right] + \frac{Gr}{R}\left[\frac{1}{s} + \frac{1-pr}{R-s(pr-1)}\right]\right] - \frac{Gm}{k}\left[\frac{1}{s} + \frac{sc-1}{k-s(sc-1)}\right] +$$
$$\frac{1}{k+\lambda}\left[\frac{1}{s-k} - \frac{1}{s+\lambda}\right] - \frac{Gr}{R}\left[\frac{e^{-y\sqrt{(J+s)pr}}}{s} - \frac{(1-pr)e^{-y\sqrt{(J+s)pr}}}{R+s(pr-1)}\right] + \frac{Gm}{k}\left[\left[\frac{e^{-y\sqrt{S\,Sc}}}{s} - \frac{(sc-1)e^{-y\sqrt{S\,Sc}}}{k-s(sc-1)}\right]\right] \quad (10)$$

$$L(\theta_c) = \frac{e^{-y\sqrt{(J+s)\,\mathrm{Pr}}}}{s} \quad (11)$$

$$L(C) = \frac{e^{-y\sqrt{(S\,Sc)}}}{s} \quad (12)$$

The desired solutions take the form:

$$u_c(y) = Cos\,\beta\left(t-\sqrt{k+s}\right) - \frac{1}{k+\lambda}e^{k\left(t-\sqrt{k+s}\right)} + \frac{1}{k+\lambda}e^{-\lambda\left(t-\sqrt{k+s}\right)}$$
$$+\left[\frac{Gr}{R}-\frac{Gm}{2k}\right]\left[e^{-y\sqrt{k}}erfc\left(\eta-\sqrt{kt}\right)+e^{y\sqrt{k}}erfc\left(\eta+\sqrt{kt}\right)\right]$$
$$-\frac{Gre^{Qt}}{2}\left[e^{-y\sqrt{Q+k}}erfc\left(\eta-\sqrt{(Q+k)t}\right)+e^{y\sqrt{Q+k}}erfc\left(\eta+\sqrt{(Q+k)t}\right)\right]$$
$$-\frac{Gm\,e^{-Dt}}{2k}\left[e^{-y\sqrt{k-D}}erfc\left(\eta-\sqrt{(k-D)t}\right)\right.$$
$$\left.+e^{y\sqrt{k-D}}erfc\left(\eta+\sqrt{(k-D)t}\right)\right]+\frac{1}{k+\lambda}\left(e^{kt}-e^{-\lambda t}\right)$$
$$-\frac{Gr}{2R}\left[e^{-y\,Pr\sqrt{J}}erfc\left[\left(\eta\sqrt{Pr}\right)-\sqrt{JPr\,t}\right]+e^{y\,Pr\sqrt{J}}erfc\left[\left(\eta\sqrt{Pr}\right)+\sqrt{JPr\,t}\right]\right]$$
$$+\frac{Gre^{Qt}}{2R}\left[e^{-y\,Pr\sqrt{J+Q}}\,erfc\left[\left(\eta\sqrt{Pr}\right)-\sqrt{(J+Q)\,\mathrm{Pr}\,t}\right]\right.$$
$$\left.+e^{y\,Pr\sqrt{J+Q}}\,erfc\left[\left(\eta\sqrt{Pr}\right)+\sqrt{(J+Q)\,\mathrm{Pr}\,t}\right]\right]$$
$$+\frac{Gm}{M}\left[erfc\left(\eta\sqrt{Sc}\right)-e^{D-\left(t-\sqrt{Sc\,S}\right)}\right] \tag{13}$$

$$\theta_c(y) = \frac{1}{2}\left\{\left[e^{-y\,Pr\sqrt{J}}\left[erfc\left(\eta\sqrt{Pr}\right)-\sqrt{JPrt}\right]+\;e^{y\,Pr\sqrt{J}}\left[erfc\left(\eta\sqrt{Pr}\right)+\sqrt{JPrt}\right]\right\} \tag{14}$$

$$C(y) = \;erfc(\eta\sqrt{Sc}) \tag{15}$$

Here the following relations apply:

$$Q=\frac{R}{Pr-1}\,,D=\frac{k}{Sc-1}\,,\beta=\alpha^2,R=(J\,Pr-k),k=\sigma^2+\frac{G_{pv}}{Re^2},\eta=\frac{y}{2\sqrt{t}} \tag{16}$$

In the next section computations in MATLAB were performed using data selected to represent CSF in hydrocephalus conditions, material properties and also various dimensionless numbers as given in **Table 1**.

Table 1: CSF data and source references

Density (kg/m^3)	0.95 [2]	Specific Heat (Cp) (J/g/K)	4.19 [2]
Thermal Conductivity (W/m/K)	0.63 [2]	Womersley Number	6.3-7.8 [16]
Permeability (m^2)	0.3	Sc, Gr, Gm	0.2, 0.39, 0.075
Pressure (Pa)	≤ 3000Pa [20]	Reynolds number	31.8 to 468.3 [19]

4. RESULTS & DISCUSSION

The purpose of this paper is to ascertain the impact of thermos solutal non-Newtonian CSF watery fluid which is shown in Figs: 2-10. The analytical solutions for velocity, temperature and concentration determined using classical Laplace and inverse transform methods are evaluated in MATLAB based on selected data in Table 1 and visualized graphically in the *Figs*. (2-10). To understand the behavior of the pulsatile flow characteristics in the hydrocephalus model, velocity (u_c),temperature(θ_c) and Concentration (C) are plotted against t for various values of different parameters such as Darcy permeability number, Schmidt number, heat conduction parameter and so on.

A strong decrement in CSF solute concentration is induced with increment in Schmidt number, as seen in Fig. 2. Since Schmidt number relates the relative rates of momentum and mass (molecular) diffusivity in the regime, higher Schmidt number implies the solute particles diffuse slower in the CSF saturated porous medium.

CSF temperature variation with various Prandtl number in different times is shown in Fig: 3. There is a significant increase in temperature observed in various Prandtl number with increment in time, implying that thermal effects are amplified as time progresses in the hydrocephalus. It elucidates for varying Prandtl number increase the thermal conduction which decrease the mass transfer. Temperature decays with increment in vertical coordinate, as one ascends the pia matter space.

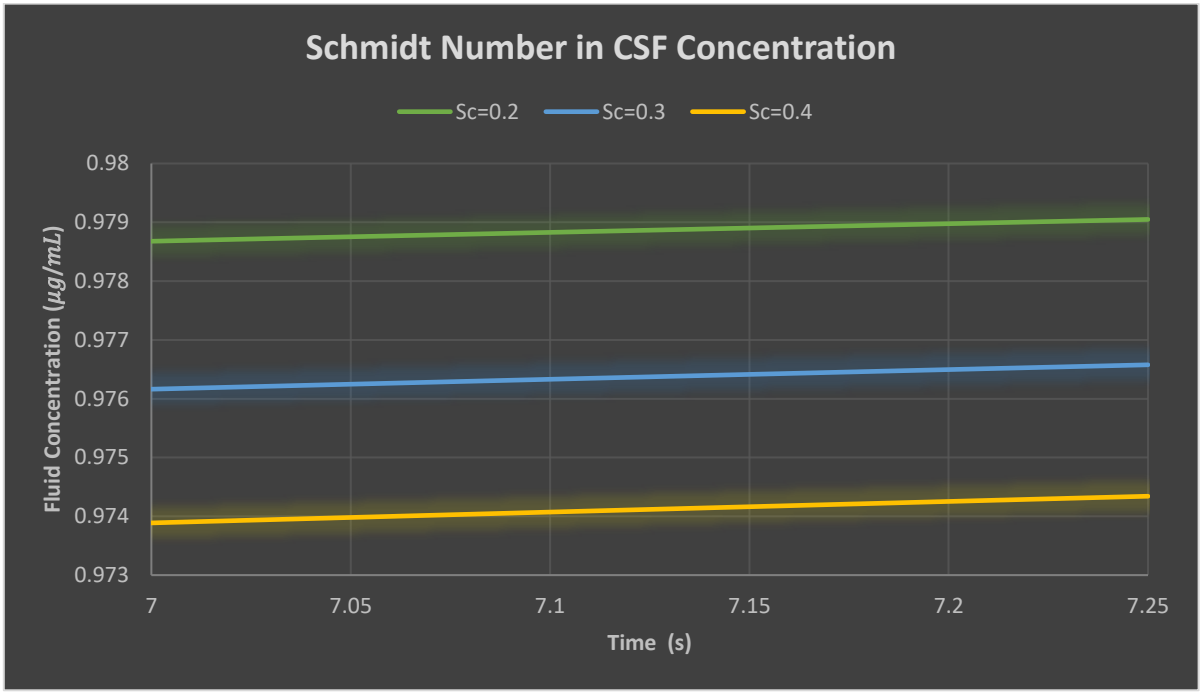

Fig.2 CSF temperature variation with Schmidt number for various times (t)

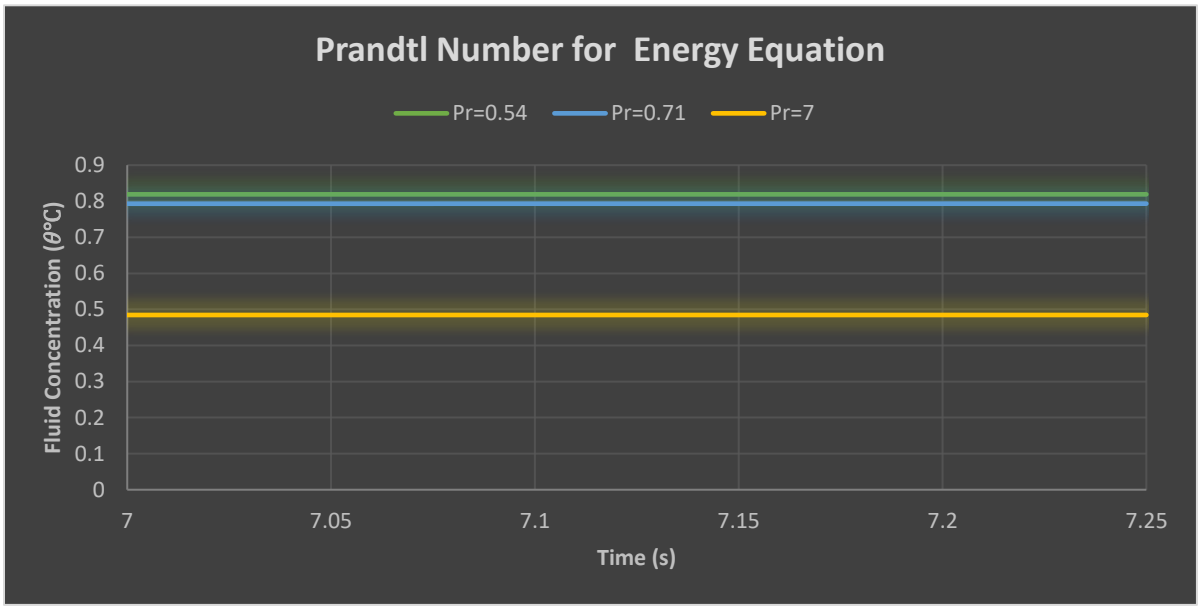

Fig: 3 CSF solute concentration variation with various Prandtl number for various time (t)

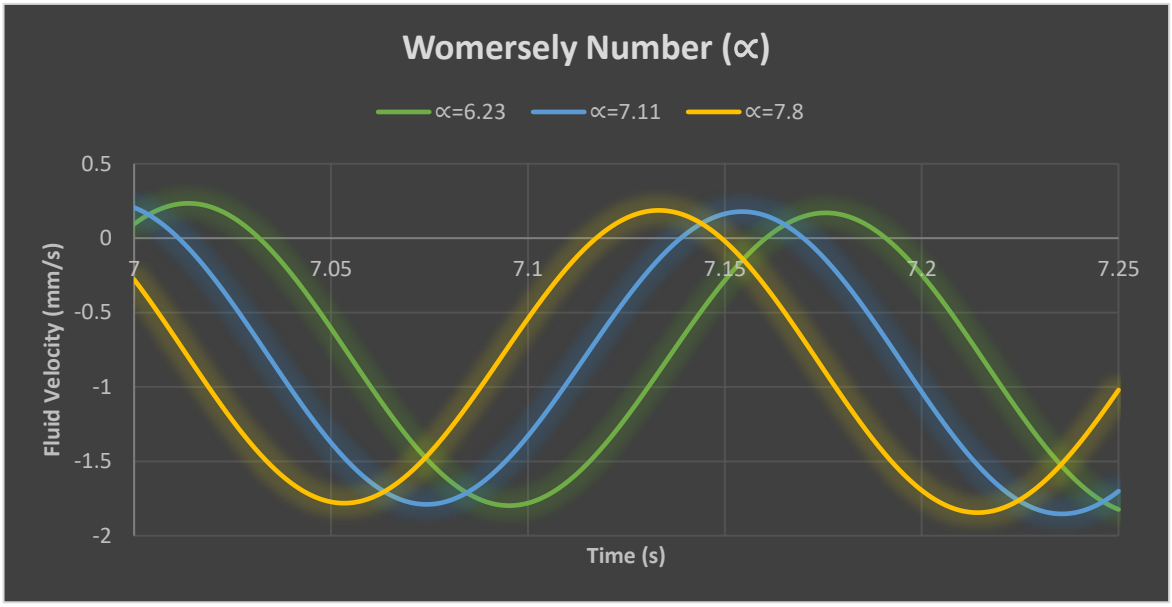

Fig: 4 CSF velocity variation with time for various Womersley number (∝)

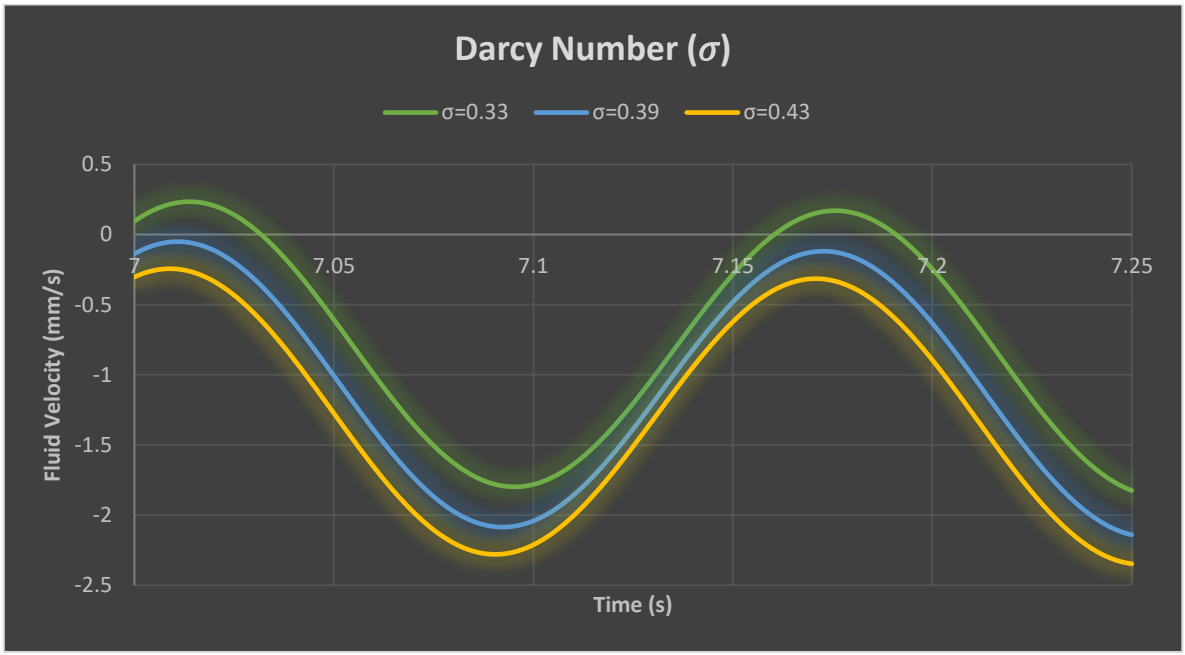

Fig: 5 CSF variation for velocity with time for various Darcy permeability (σ)numbers

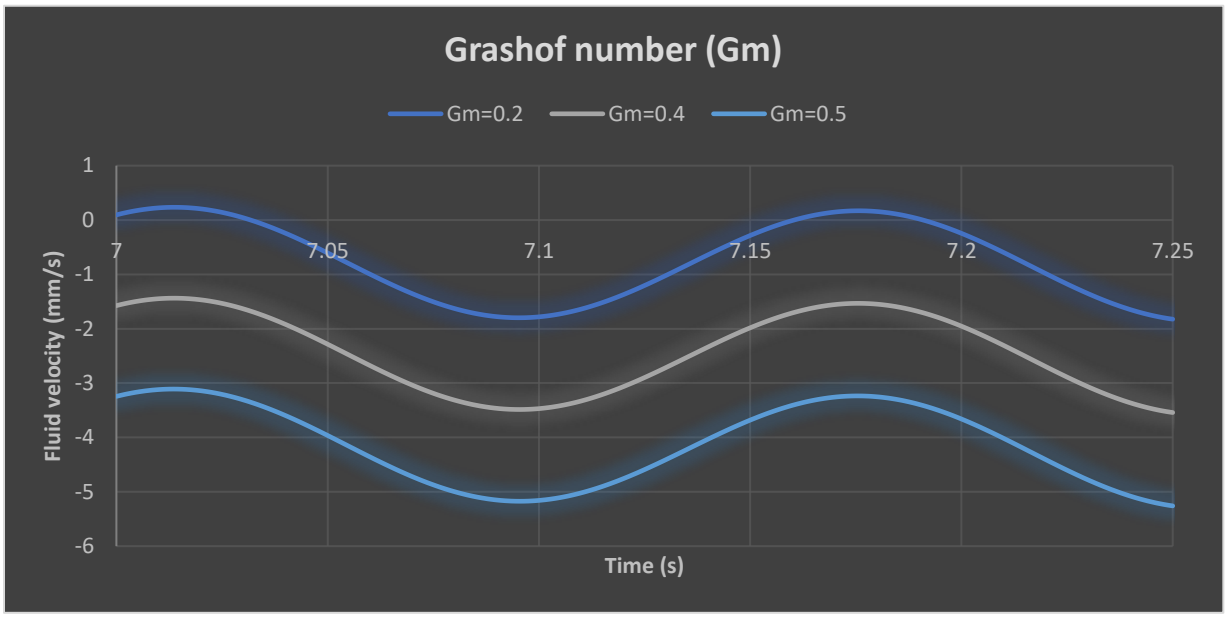

Fig: 6 CSF variation for velocity with time for various Grashof numbers for mass transfer.

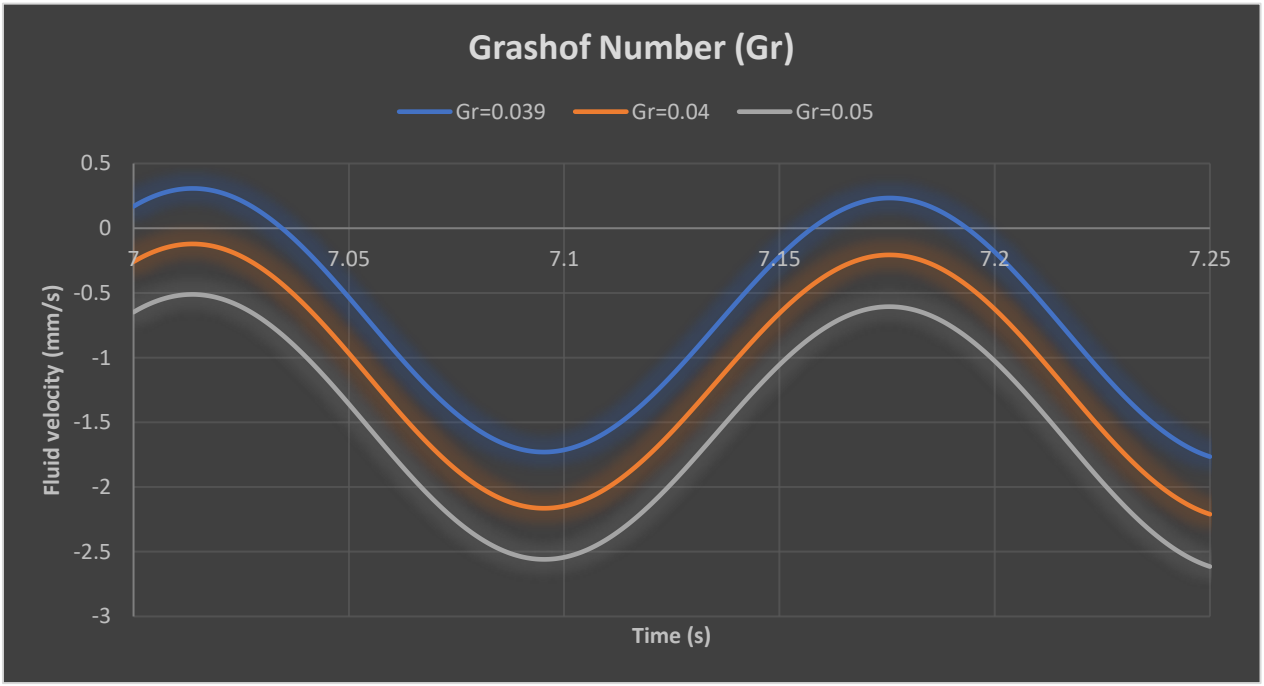

Fig: 7 CSF variation for velocity with time for various thermal Grashof numbers (Extra Graph added)

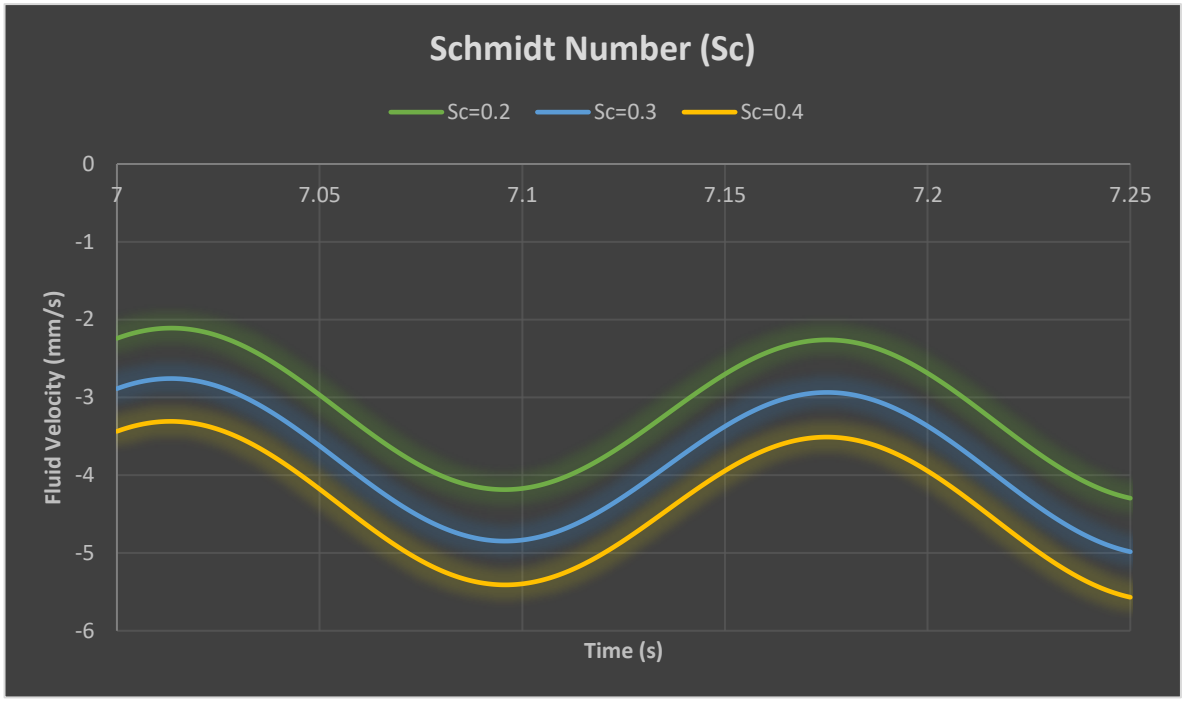

Fig: 8 CSF for velocity with time for various Schmidt numbers

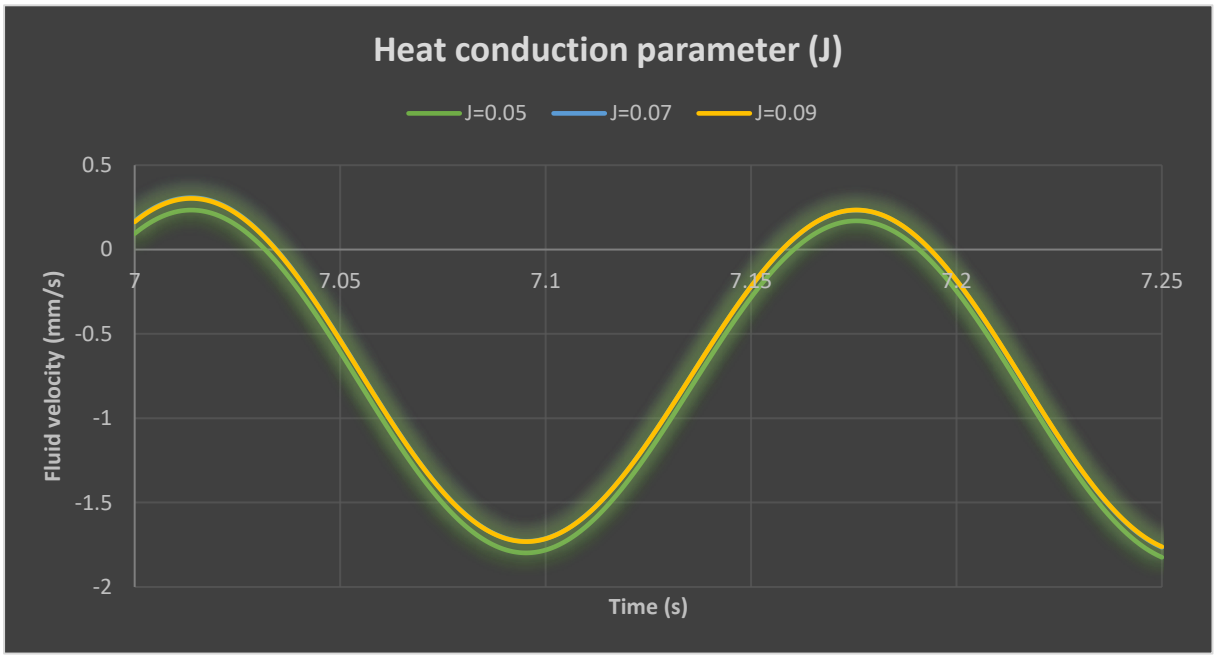

Fig: 9 CSF for velocity with time for various heat conduction parameters

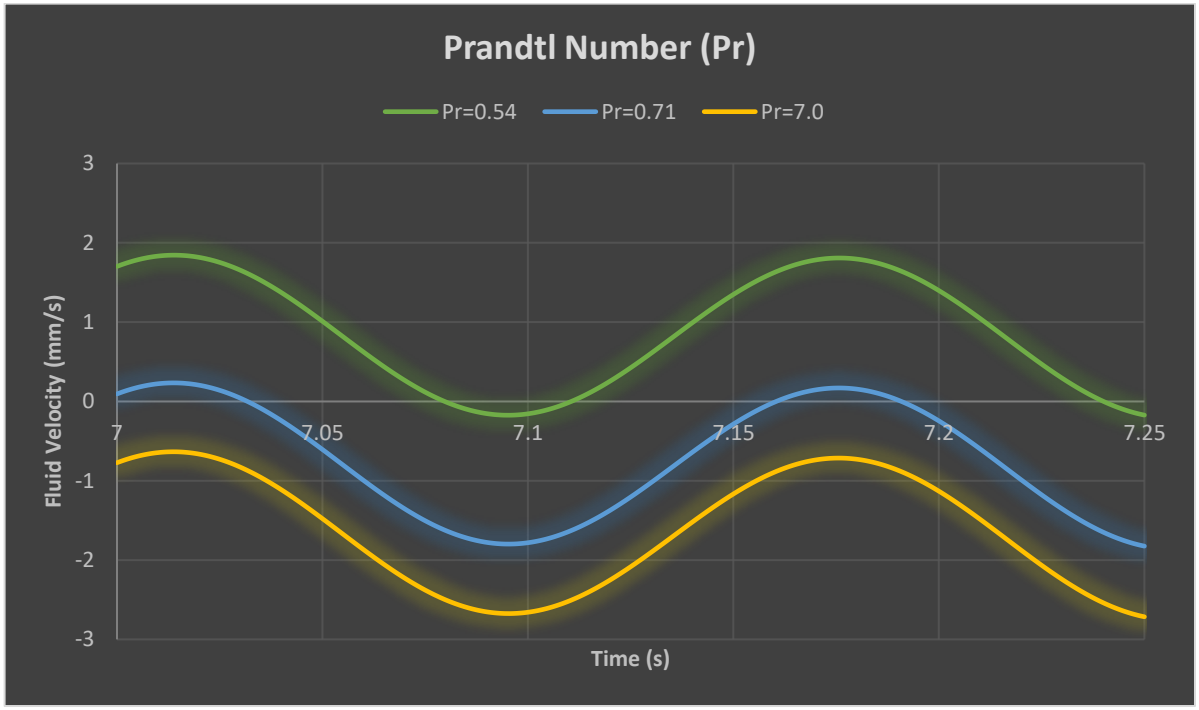

Fig: 10 CSF for velocity with time for various Prandtl numbers.

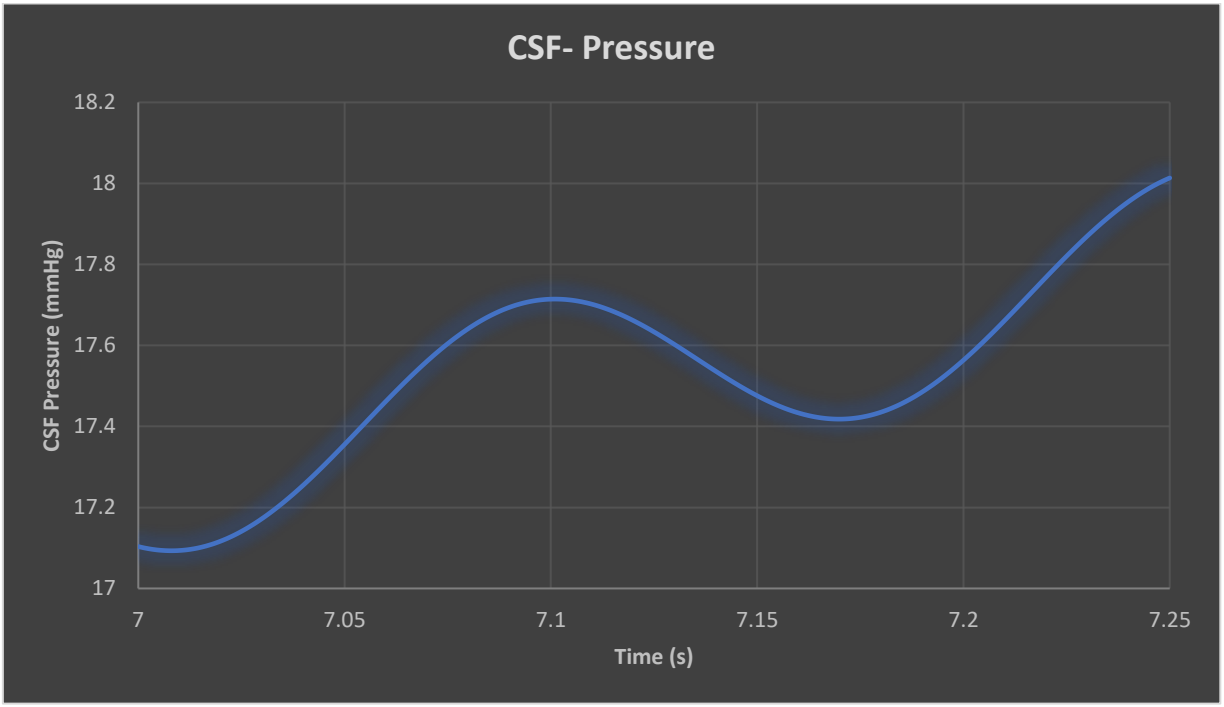

Fig: 11 CSF pressure with time variation for hydrocephalus patients

Fig. 4 shows that a strongly periodic (oscillatory) profile of the CSF flow has been captured. As Womersley number increases, the inertial force grows relative to the viscous (damping) force. This displaces the peak values of CSF velocity and also the troughs (minimal values), although magnitudes generally remain the same. The effect of time elapse is that pulsatile waves are displaced which is linked to the periodic nature of the flow.

In Fig. 5, the CSF velocity is observed to be reduced with Darcy permeability parameter. In Eqn. (7), the Darcian body force, $-\sigma^2 u_c$, is a negative (drag) force exerted by the solid fibers in the pia matter on the CSF. However, since $\sigma^2 = \frac{\nu^2}{{U_0}^2 k_{m^*}}$ this force is inversely proportional to the permeability. As σ^2 increases the permeability is clearly reduced, implying that greater resistance is exerted on the percolating CSF flow. This damps the flow ~~i.e~~ induces deceleration and manifests in a decrease in CSF velocity. Furthermore, the pulsating nature of the CSF flow is clearly captured with time variation in Fig. 5.

Figures 6 and 7 display the influence of the Grashof number in heat transfer and solutal mass transfer Gm respectively. Fig 6 illustrates the increase in Grashof numbers considerably escalates the fluid flow with decreasing CSF velocities. On the other way, In Fig. 7, a significant depletion in CSF flow velocity is computed with increment in thermal Grashof number. Gr arises in the momentum Eqn. (7) and couples the velocity and temperature field. Increasing thermal buoyancy is induced with higher values of *Gr* but this acts to damp the CSF flow in the regime.

Fig. 8 shows the impact of Schmidt number on oscillatory CSF velocity profiles plotted against time. The peaks are displaced clearly with time progression; however, the magnitudes of these peaks are not tangibly altered with Schmidt number. In Fig. 9 there is a strong decrement observed in CSF velocity with increasing heat conduction parameter (*J*). CSF velocity is also observed to decrease with elapse in time. Stronger heat conduction in the regime results in flow deceleration and this indicates that, if thermal effects are neglected in the simulations, erroneous results are obtained. It is therefore important to include thermal effects in realistic models of CSF hydrocephalus transport.

In Fig. 10, We display the effect of Prandtl number in CSF temperature profiles in figures 00 and 00 with respect to time variation. It is understood that the increase in heat conduction parameter result in increase to heat diffusivity. Therefore, it is observed that an increase in the Prandtl number results in

decrease in the thermal boundary SAS layer thickness which slow down the average temperature within the wall of SAS layer. In this simulation, the values of Prandtl number used are 7.0, 0.54 and 0.71 corresponds to the molecules of CSF with water, CSF and air respectively.

Finally, Fig. 11 shows that CSF pressure remains largely invariant at values increase in time values; however, after significant elapse in time, there is a strong elevation in the pressure computed. As the fluid flow increases in the subarachnoid space, a significant amount of fluid passes through the brain parenchyma and the pressure of the fluid escalates drastically due to hydrocephalus disorder. Interesting observations have been made of the thermal, solute (e. g. ion) and also velocity distributions in pulsating CSF flow in the hydrocephalus. Ions in the excess fluid diffuse strongly and this also contributes to excess molecules in this pathophysiological disorder.

5. CONCLUSIONS

A theoretical study has been presented for pulsatile flow in a porous medium model of the hydrocephalus with combined heat and mass transfer. Thermal and mass (solutal) buoyancy effects have been included. Darcy's model is deployed for the pia matter (porous medium). The non-dimensional model is solved using Laplace transforms with error functions. Graphical results are then presented with clinically viable data using MATLAB symbolic software for the influence of selected emerging transport parameters.

The analysis reveals ~~that~~ with increasing permeability of the subarachnoid space, the CSF velocity is increased, and a significant fluid flux enhancement arises through the brain parenchyma as the pressure of the fluid escalates drastically due to hydrocephalus disorder. Stronger thermal buoyancy (Grashof number) also results in deceleration in the flow. CSF temperature is reduced with progression in time. Solute concentration (e.g. ions) is suppressed with increasing Schmidt number. As heat conduction parameter increases there is a substantial depletion in CSF velocity with respect to time.

As Womersley number is elevated the inertial force grows relative to the viscous (damping) force and this displaces the peak values of CSF velocity and also the troughs (minimal values), although magnitudes generally remain the same. CSF pressure remains largely invariant at lower time values; however, after significant elapse in time, there is a strong elevation in the pressure computed. As the fluid flow increases in the subarachnoid space, a significant amount of fluid passes through the brain

parenchyma and the pressure of the fluid escalates drastically due to hydrocephalus disorder with associated ventricular enlargement. The present study has revealed some interesting features of thermo-solutal transport in an idealized model of the hydrocephalus of relevance to neurological medicine. The following were the conclusions that were made from the present investigation.

- ✓ The velocity of a fluid flow decreases for increasing Prandtl number, heat conduction parameter and Schmidt number.
- ✓ Increase in Darcy number, Grashof number of mass transfer, Grashof number of heat transfer with respect to time results in increase in CSF velocity.
- ✓ There is a significant change in temperature fall due to the enhancement of heat conduction parameter and Prandtl number.
- ✓ Impact of increase in Schmidt number considerably reduces the fluid concentration.
- ✓ Increase in fluid velocity reflects significant changes in high intracranial pressure in the flow regime.

Future works may generalize the present approach to consider non-Newtonian characteristics of CSF and more complex geometries.

6. REFERENCES

1. Hirashima, Yutaka, Michiyasu Takaba, Shunro Endo, Nakamasa Hayashi, Kazuhiko Yamashita, and Akira Takaku. "Intracerebral temperature in patients with hydrocephalus of varying aetiology." *Journal of Neurology, Neurosurgery & Psychiatry* 64, no. 6: 792-794. (1998)
2. Rajasekaran, Sathish, Hongwei Qu, and Karol Zakalik. "Thermal measurement of cerebrospinal fluid flow rate in hydrocephalus shunt." In *2015 IEEE SENSORS*, pp. 1-4. IEEE, (2015).
3. Madsen, Joseph R., Gani S. Abazi, Laurel Fleming, Mark Proctor, Ron Grondin, Suresh Magge, Peter Casey, and Tomer Anor. "Evaluation of the ShuntCheck noninvasive thermal technique for shunt flow detection in hydrocephalic patients". *Neurosurgery* 68, no. 1: 198-205. (2011)
4. Neff, Samuel. "Measurement of flow of cerebrospinal fluid in shunts by transcutaneous thermal convection." *Journal of Neurosurgery: Pediatrics* 103, no. 4: 366-373. (2005)
5. Herbowski, Leszek, and Henryk Gurgul. "Thermodynamic Approach to Cerebrospinal Fluid Circulation." *Journal of Neurology Research* 1, no. 5: 215-218. (2011)

6. Déli, Eva, and Zoltán Kisvárday. "The thermodynamic brain and the evolution of intellect: the role of mental energy." *Cognitive Neurodynamics* : 1-14. (2020)
7. Donnelly, Joseph, and Marek Czosnyka. "The thermodynamic brain." *Critical Care* 18, no. 6: 1-2. (2014)
8. Zakharov, Michael, and Michael Sadovsky. "The role of blood circulatory system in thermal regulation of animals explained by entropy production analysis." *arXiv preprint arXiv:1308.3663*. (2013)
9. Gholampour, S., N. Fatouraee, A. S. Seddighi, and A. Seddighi. "Numerical simulation of cerebrospinal fluid hydrodynamics in the healing process of hydrocephalus patients." *Journal of Applied Mechanics and Technical Physics* 58, no. 3: 386-391. (2017)
10. Keong, Nicole C., Alonso Pena, Stephen J. Price, Marek Czosnyka, Zofia Czosnyka, Elise E. DeVito, Charlotte R. Housden, Barbara J. Sahakian, and John D. Pickard. "Diffusion tensor imaging profiles reveal specific neural tract distortion in normal pressure hydrocephalus." *PloS one* 12, no. 8: e0181624. (2017)
11. McAllister, James P., Michael A. Williams, Marion L. Walker, John RW Kestle, Norman R. Relkin, Amy M. Anderson, Paul H. Gross, and Samuel R. Browd. Opportunities for hydrocephalus research: pathways to better outcomes, *Journal of Neurosurgery*, 123, no. 6: 1427-1438. (2015)
12. A. Smillie , I. Sobey & Z. Molnar , A hydro-elastic model of hydrocephalus, Report no. 04/03, *Oxford University Computing Laboratory Numerical Analysis Group Wolfson Building Parks Road Oxford, England, February* (2004).
13. David C. Zhu, Michalis Xenos, Andreas A. Linninger, and Richard D. Penn, MD “Dynamics of Lateral Ventricle and Cerebrospinal Fluid in Normal and Hydrocephalic Brains” *Journal of Magnetic Resonance Imaging* 24:756 –770 (2006)
14. K.M. Tangen *et al.*, CNS wide simulation of flow resistance and drug transport due to spinal microanatomy, *Journal of Biomechanics* 48 (2015) 2144–2154.
15. Gholampour S. FSI simulation of CSF hydrodynamic changes in a large population of non-communicating hydrocephalus patients during treatment process with regard to their clinical symptoms. *PLoS One*. 2018;13(4):e0196216. (2018). doi:10.1371/journal.pone.
16. Balasundaram, H.; Sathiamoorthy, S.; Santra, S.S.; Ali, R.; Govindan, V.; Dreglea, A.; Noeiaghdam, S. Effect of ventricular elasticity due to congenital hydrocephalus. *Symmetry* 2021, *13*, 2087. https://doi.org/10.3390/sym13112087

17. Gholampour, Seifollah, and Nasser Fatouraee. "Boundary conditions investigation to improve computer simulation of cerebrospinal fluid dynamics in hydrocephalus patients." *Communications biology* 4.1 (2021): 1-15.
18. Gholampour S *et al.* Evaluating the effect of hydrocephalus cause on the manner of changes in the effective parameters and clinical symptoms of the disease. *J Clin Neurosci* (2016), http://dx.doi.org/10.1016/j.jocn.2016.09.012
19. Gholampour S, Bahmani M. Hydrodynamic comparison of shunt and endoscopic third ventriculostomy in adult hydrocephalus using in vitro models and fluid-structure interaction simulation. *Computer Methods and Programs in Biomedicine*. 2021, 1; 204: 106049.
20. J. Malm, B. Kristensen, M. Fagerlund, *et al.*, "Cerebrospinal fluid shunt dynamics in patients with idiopathic adult hydrocephalus syndrome," *J. Neurology, Neurosurgery Psychiatry* 67, 273–277 (2009).
21. A. A. Linninger, M. Xenos, D. C. Zhu, et al., "Cerebrospinal fluid flow in the normal and hydrocephalic human brain," *IEEE Trans. Biomed. Engng*. 54, 291–302 (2007).
22. B. Sweetman, M. Xenos, L. Zitella, and A. A. Linninger, "Three-dimensional computational prediction of cerebrospinal fluid flow in the human brain", *Comput. Biol. Med.* 41, 67–75 (2011).
23. Hetnarski R., On inverting Laplace transform connected with the error function. *Applications Mathematics 7.4: 399-409* (1964).
24. Bhatti, M. M., et al. "Sinusoidal motion of small particles through a Darcy-Brinkman-Forchheimer microchannel filled with non-Newtonian fluid under electro-osmotic forces." *Journal of Taibah University for Science* 15.1 (2021): 514-529.
25. Majeed, Aaqib, Ahmad Zeeshan, and Farzan Majeed Noori. "Analysis of chemically reactive species with mixed convection and Darcy–Forchheimer flow under activation energy: a novel application for geothermal reservoirs." *Journal of Thermal Analysis and Calorimetry* 140.5 (2020): 2357-2367.
26. Majeed, A., A. Zeeshan, and F. M. Noori. "Numerical study of Darcy-Forchheimer model with activation energy subject to chemically reactive species and momentum slip of order two." *AIP Advances* 9.4 (2019): 045035.
27. Zeeshan, Ahmad, Muhammad Muddassar Maskeen, and Obaid Ullah Mehmood. "Hydromagnetic nanofluid flow past a stretching cylinder embedded in non-Darcian Forchheimer porous media." *Neural Computing and Applications* 30.11 (2018): 3479-3489.

28. Shehzad, Nasir, et al. "Modelling study on internal energy loss due to entropy generation for non-Darcy Poiseuille flow of silver-water nanofluid: an application of purification." *Entropy* 20.11 (2018): 851.
29. Gutiérrez-Montes, C., et al. "Modelling and direct numerical simulation of flow and solute dispersion in the spinal subarachnoid space." *Applied Mathematical Modelling* 94 (2021): 516-533.

ACKNOWLEDGMENTS:

The authors thank Prof. R Muthucumaraswamy, Dean and Head, SVCE College for his kind support with the present research.

CONFLICTS OF INTEREST:

The authors declare no conflict of interest.